Receptive field structure of H1 horizontal cells in macaque monkey retina

Orin S. Packer
Department of Biological Structure, University of Washington, Seattle, WA, USA

Dennis M. Dacey
Department of Biological Structure, University of Washington, Seattle, WA, USA

The ganglion cells of primate retina have center-surround receptive fields. A strong candidate for mediating linear surround circuitry is negative feedback from the H1 horizontal cell onto the cone pedicle. We measured the spatial properties of H1 cell receptive fields in the in vitro macaque monkey retina using sinusoidal gratings, spots, and annuli. Spatial tuning curves ranged in shape from smoothly low pass to prominently notched. The tuning curves of ~80% of cells could be well described by a sum of two exponentials, giving a prominent central peak superimposed on a broad shallow skirt. The mean diameter of the combined receptive field decreased with eccentricity from 309 μm at 11 mm to 122 μm at 4 mm. We propose that the strong narrow field reflects direct synaptic input from the cones overlying the dendritic tree whereas the weak wide field reflects coupled inputs from neighboring H1 cells. Those cells not well fit by a sum of exponentials had tuning curves with additional peaks at higher spatial frequencies that were likely due to undersampling in the cone-H1 network. Unlike other vertebrates, the macaque H1 network is less strongly coupled, has smaller receptive fields, and shows no functional plasticity. Macaque H1 receptive fields are surprisingly small, suggesting a great reduction in electrical coupling. Because the center of the H1 receptive field gets only a small percentage of its total response from the coupled field, the smallest receptive fields are similar in diameter to the dendritic trees. They are probably small enough to form the surrounds of foveal midget cells. The H1 network is compatible with a mixed-surround model of spectral opponency.

Keywords: H1 horizontal cells, macaque, retina, receptive fields, physiology, anatomy

Introduction

The midget pathway of the primate fovea is specialized to transmit both spatial and chromatic signals. Many features of the underlying circuitry are well understood (Polyak, 1941; Kolb & Dekorver, 1991). A midget bipolar cell gets center input from a single cone and transmits the cone signal to the dendritic tree of a single midget ganglion cell (Calkins, Schein, Tsukamoto, & Sterling, 1994). As a result of this "private line" pathway, the receptive field center inherits the small diameter of the cone receptive field preserving the high spatial resolution afforded by the photoreceptor mosaic (Lee, Kremers, & Yeh, 1998; McMahon, Lankheet, Lennie, & Williams, 2000). The private line circuit also confers red/green spectral opponency. Red/green opponency occurs when L and M cone signals to the receptive field are antagonistic and thus dependent on an inhibitory surround pathway. Although the pure cone receptive field center is a consequence of the private-line anatomy, the circuitry that mediates the structure and cone composition of the surround is not well understood (Dacey, 1999).

Ganglion cell surrounds are a complicated combination of linear and nonlinear components (Kaplan & Benardete, 2001; Benardete & Kaplan, 1997a; Benardete & Kaplan, 1997b). The linear component of the midget cell surround is likely mediated by H1 horizontal cells whose graded response to light is itself quite linear (Smith, Pokorny, Lee, & Dacey, 2001). The nonlinear component may be mediated by long distance inputs from spiking amacrine cells (Taylor, 1999; Demb, Haarsma, Freed, & Sterling, 1999). H1 cells in macaque contact L and M cones (Dacheux & Raviola, 1990) and avoid contact with S cones (Dacey, Lee, Stafford, Pokorny, & Smith, 1996). Like the horizontal cells of other vertebrates (Werblin & Dowling, 1969; Naka & Nye, 1971; Kaneko, 1970; Naka & Witkovsky, 1972; Baylor, Fuortes, & O'Bryan, 1971; Mangel, 1991), the H1 cell likely provides a feedback signal (Kamermans & Spekreijse, 1999) that generates a surround in cones (Julie Schnapf, personal communication, 2002) and bipolar cells (Dacey, Packer, Diller, Brainard, Peterson, & Lee, 2000). To form foveal midget surrounds, horizontal cell receptive fields must be no larger than midget ganglion cell surrounds (de Monasterio, 1978; Reid & Shapley, 1992) whose diameter can be as small as 20 to 30 μm (Lee et al., 1998; Croner & Kaplan, 1995).

Can primate H1 cells mediate the small inhibitory surrounds of the midget pathway? Not if they are similar to the horizontal cells of other vertebrates. Non-

DOI 10:1167/2.4.1 Received January 31, 2002; published June 17, 2002 ISSN 1534-7362

mammalian horizontal cells have such extensive electrical coupling (Yamada & Ishikawa, 1965; Kaneko, 1971; Witkovsky, Owen, & Woodworth, 1983; Naka & Rushton, 1967; Lamb, 1976) mediated by gap junctions among their dendrites that horizontal cell receptive fields can span most of the retina (Tornqvist, Yang, & Dowling, 1988). The horizontal cells of mammalian retinas, such as those in cat and rabbit, are also extensively coupled and consequently have uniformly large receptive fields (Mills & Massey, 1994; Bloomfield, Xin, & Persky, 1995). However, the anatomy of the primate H1 network strongly suggests unique functional specializations. H1 cell morphology depends strongly on eccentricity. Density increases by a factor of 25 from the periphery (~1,000 cells/mm^2) to the fovea (~25,000 H1 cells/mm^2 at 1 mm of eccentricity) (Wässle et al., 2000). Dendritic field diameter decreases by a factor of 10 (160 μm to 16 μm diameter) (Figure 1) (Wässle, Boycott, & Rohrenbeck, 1989). In fact, dendritic field size decreases so much faster than density increases that the number of overlapping dendritic fields (coverage) decreases by a factor of 10 (30 in far periphery, 3 near the fovea) (Wässle et al., 2000). As a result, foveal cells have small, largely non-overlapping dendritic trees quite different from the large, highly overlapping trees of peripheral cells. To what degree are these anatomical gradients reflected in the physiology? If receptive fields scale with eccentricity as dendritic trees do, central H1 receptive fields will be small. Just how small depends on whether coupling decreases as dendritic overlap decreases. If it does, central H1 receptive fields can be small enough to form foveal midget surrounds.

Can primate H1 cells mediate spectral opponency? The selective circuitry needed to produce a pure cone surround does not exist in the primate H1 network (Dacey et al., 1996; Dacey, Diller, et al., 2000). However, opponency is created even when horizontal cells indiscriminately sum L and M cones (Lennie, Haake, & Williams, 1991) to create surrounds that have uniform L/M cone input ratios similar to that of the cone mosaic as a whole. If foveal midget cells have surrounds small enough to take advantage of the patchy distribution of L and M cones (Packer, Williams, & Bensinger, 1996; Roorda, Metha, Lennie, & Williams, 2001), increased opponency might result from the formation of surrounds with nonuniform L/M ratios, including at least a few pure cone surrounds.

To explore these questions, we measured the spatial properties of H1 horizontal cell receptive fields in the in vitro macaque monkey retina (Dacey & Lee, 1994; Dacey et al., 1996). Consistent with a strong correlation between anatomy and physiology, H1 receptive field diameter was strongly eccentricity dependent. At all eccentricities, receptive fields were relatively small compared with those of other vertebrates, suggesting relatively weak coupling. H1 receptive fields were surprisingly complex, requiring the development of a multicomponent model to predict receptive field sensitivity. We used this model to examine the implications of horizontal cell specialization on receptive field organization and spectral opponency.

Methods

Tissue Preparation

Macaque monkey (*Macaca nemestrina, M. fascicularis)* and baboon (*Papio c. anubis)* retinas were obtained through the tissue program of the University of Washington Regional Primate Center, Seattle, WA. Tissue preparation was previously described (Dacey & Lee, 1994; Dacey et al., 1996). In brief, the retina, choroid, and pigment epithelium were dissected as a unit from the vitreous and sclera and placed in oxygenated Ames medium (Sigma, St. Louis, MO). They were mounted vitreal side up in a superfusion chamber fixed to a microscope stage. H1 horizontal cell nuclei stained with 4,6 diamidino-2-phenylindole (DAPI) (10 μM) were identified under the microscope by their large granular nuclei just vitreal to the photoreceptor nuclei. Targeted cells were penetrated with glass microelectrodes filled with 3% biocytin and 2% pyranine in 1M KCl or 1M K acetate. Electrode impedance exceeded 200 MΩ. After penetration, cell type was confirmed by the characteristic hyperpolarizing light response (Smith et al., 2001) as well as by iontophoresis of pyranine, whose fluorescence revealed their dendritic morphology.

After recording, images of illuminated cells were collected using a charge coupled device (CCD) camera attached to the camera port of the microscope. Some cells were filled with biocytin-X-hydrazide (Molecular Probes, Eugene, OR) by iontophoresis through the recording electrode (0.1 - 0.5 nA for 10-30 min). This tracer does not easily cross gap junctions and is ideal for filling single cells (Mills & Massey, 2000). At the end of the experiment, the retina was dissected from the retinal pigment epithelium and choroid, fixed in phosphate buffered 4% paraformaldehyde for 2 hr, and stored in phosphate buffer (pH 7.4). Standard horseradish peroxidase histochemistry converted the tracer into a black reaction product. The retina was mounted on a slide using a solution of polyvinyl alcohol and glycerol. Tracings of H1 horizontal cells were made from photographic images or using a microscope drawing tube. Images of Golgi stained cells were photographed from whole mounted retinas donated to the laboratory by R.W. Rodieck.

Stimuli and Data Acquisition

Spots, annuli, and sine wave gratings were created using a stimulator based on a digital light projector (Packer et al., 2001). These patterns were relayed by an optical system to the camera port of the microscope and imaged on the retina by a microscope objective.

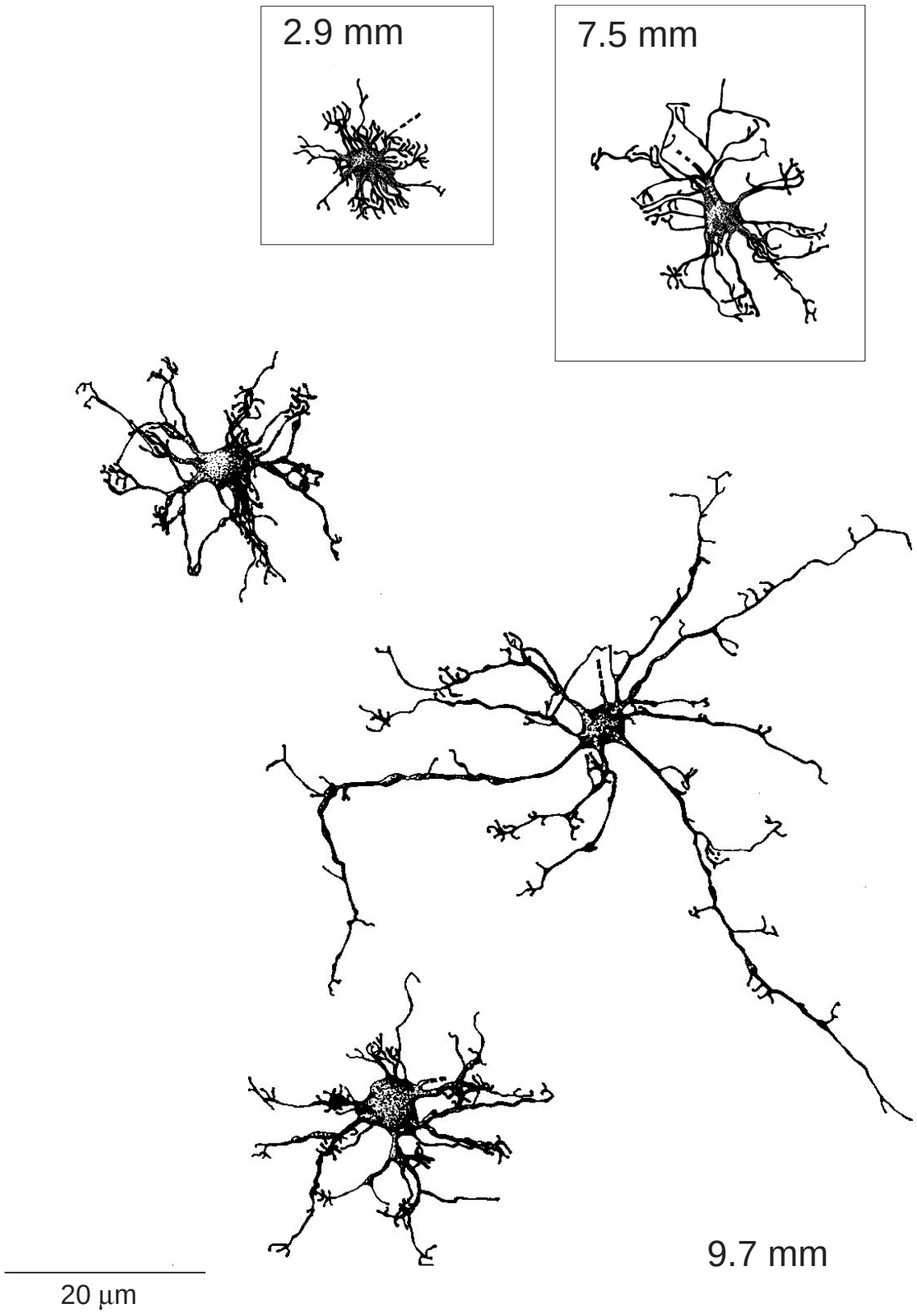

Figure 1. Tracings of Golgi stained H1 horizontal cells from macaque monkey retina. The eccentricity (mm) of the cells is shown with each drawing. The two cells at the bottom were neighboring cells in the same retina at the same eccentricity. The scale bar indicates distance.

H1 horizontal cell receptive fields were characterized by measuring their responses to drifting sinusoidal gratings as a function of spatial frequency, to flashing spots as a function of spot diameter, and to flashing annuli as a function of annulus inner diameter. The receptive field center was found by moving a small flickering spot of light across the retina to the location of maximum response. Temporal frequency was 2, 4, or 10 Hz. Stimulus contrast was nominally 5, 10, 25, 50, or 100%. Ideally, a 100% contrast grating would have 100% contrast at all spatial frequencies. In fact, a reduction in the contrast of grating stimuli at higher spatial frequencies was introduced by the visual stimulator (Packer et al., 2001). This was corrected by multiplying the response by the inverse of the contrast sensitivity function of the stimulator at that spatial frequency. The validity of this correction, which depends on linear contrast response by the H1 cell, was verified experimentally. Unless otherwise stated, stimuli were modulated around a mid-photopic luminance of ~1,000 trolands (167 cd/m^2, 6 mm pupil) to maintain a stable state of adaptation. The relative strengths of the L and M cone inputs to many cells were measured with a stimulus (Dacey, Diller, et al., 2000) that varied the ratio of L and M cone contrasts over a wide range from pure L cone contrast through equal L and M cone contrasts to pure M cone contrast. A few cells were also tested with a stimulus designed to stimulate L, M, and S cones in isolation.

The intracellular voltage response to a stimulus was amplified (Axoprobe-1A; Axon Instruments, Foster City, CA), digitized (NBIO16 installed in a Macintosh computer; National Instruments, Austin, TX) at a sampling rate of up to 10 kHz, and averaged over multiple stimulus cycles. The amplitude and phase of the response at the temporal frequency of stimulus modulation were calculated using a digital Fourier transform.

Modeling

The horizontal cell network of nonmammalian vertebrates has traditionally been modeled as a thin sheet of cytoplasm of infinite lateral extent bounded by cell membranes (Naka and Rushton, 1967). When this infinite sheet is stimulated by inputs from photoreceptors, voltage decays exponentially from the point of stimulation. Lamb (1976) derived explicit response predictions for specific stimulus configurations. Because we made most of our measurements with drifting gratings, we initially intended to compare our responses to the Fourier transforms of line weighting functions. The line weighting function measured in the space domain using a long thin bar is essentially equivalent to the Fourier transform of the modulation transfer function measured in the frequency domain with drifting gratings. However, it became immediately apparent (see "Results") that the majority of the spatial tuning functions had shoulders and/or multiple peaks that are incompatible with a single exponential model.

The H1 spatial tuning curves measured in this paper were fit using the Enroth-Cugell et al. (1983) model of the receptive field that takes into account both the amplitude and phase of the response. Responses to spots and annuli were fit using the same underlying model. Although this model was developed for fitting an antagonistic center-surround receptive field whose center and surround were Gaussian in shape, it can also be used to fit a two-component receptive field whose responses sum. The details of our previous use of this model to fit center-surround receptive fields are given elsewhere (Dacey, Packer, et al., 2000). For use with horizontal cells, the model was modified (Dave Brainard, personal communication) so that responses could be fit with exponential as well as Gaussian functions. The wide exponential component of the receptive field has a radial profile $L(r)$ given by

$$L(r) = W_L \exp(-2.3r / R_L) \quad (1)$$

where W_L specifies the strength and R_L specifies the radius at 0.1 of peak value. A similar expression defines the narrow component $S(r)$ with strength W_S and radius R_S. The amplitudes of the narrow and wide components are calculated from the two-dimensional spatial integral of the product of the appropriate receptive field profiles. The overall amplitude and phase of the response are obtained by combining the two components:

$$R = A_L \exp(i\theta_L) + A_S \exp(i\theta_S) = A \exp(i\theta) \quad (2)$$

where A_L and A_S represent the amplitudes of the narrow and wide components and θ_L and θ_S represent their phases at the temporal frequency of stimulus modulation.

Because H1 receptive field sensitivity profiles are smooth, there is no single correct location at which to measure receptive field diameter. Ganglion cell receptive field sensitivity profiles fit with Gaussians are commonly measured at 1/e (0.36) of maximum sensitivity. However, the exponentials used to fit H1 receptive fields fall faster with increasing distance from the receptive field center than do Gaussians. As a result, many H1 receptive field diameters measured at 1/e of peak sensitivity were smaller than the dendritic tree. To avoid this improbable outcome, all measurements of receptive field diameter were made at 0.1 of peak sensitivity, the criterion at which the smallest receptive fields and dendritic trees were similar in size.

Results

Receptive Field Structure of H1 Horizontal Cells

Responses to gratings, spots, annuli

Receptive fields were characterized using drifting sinusoidal gratings. Both the amplitude and phase of the response at the temporal drift frequency were measured. A spatial tuning curve (Figure 2a) was created by plotting the fundamental amplitude of the response as a function of spatial frequency. H1 cells responded best to low spatial frequencies and increasingly less well to spatial frequencies up to ~0.04 cycles/μm (8 cycles/degree). Spatial tuning curves were fit using the modified Enroth-Cugell, Robson, Schweitzer-Tong, and Watson (1983) model (see "Methods"). The data were best fit by a sum of two exponentials (see next section).

The receptive field characteristics of a subset of the cells were also measured using a centered spot (Barlow, 1957) or annulus while systematically varying diameter. For each spot outer diameter or annulus inner diameter, the amplitude and phase of the response at the temporal modulation frequency were measured. When stimulated with a spot of increasing diameter (Figure 2b, solid symbols), the response increased until spot diameter equaled receptive field diameter. Larger spots produced no further response increase. When stimulated by an annulus whose outer diameter was larger than that of the receptive field (Figure 2c, solid symbols), the response was maximized when inner diameter was small and the entire receptive field was stimulated. As inner diameter increased, the response decreased. When inner diameter exceeded the diameter of the receptive field, the cell no longer responded. Area and annulus summation functions were fit with the same model used with drifting gratings.

The three types of stimuli produced similar estimates of spatial receptive field properties. As with gratings, the responses to spots and annuli were best fit by a sum of two exponentials. To compare responses to the three types of stimuli, we calculated the receptive field profiles (Figure 2d) that were most consistent with the area and annulus response curves (Figure 2b,c). For drifting gratings, the receptive field profile was the Fourier transform of the spatial tuning curve (Figure 2a). The receptive field profiles were normalized to peak value to factor out small changes in cell responsiveness. Receptive field diameters estimated from the responses to gratings (solid line), spots (dotted line), and annuli (dashed line) were quite similar (154, 103, and 117 μm, respectively). A total of 21 cells were measured with at least two different stimuli. Absolute differences in receptive field size from cell to cell were eliminated by calculating diameter ratios

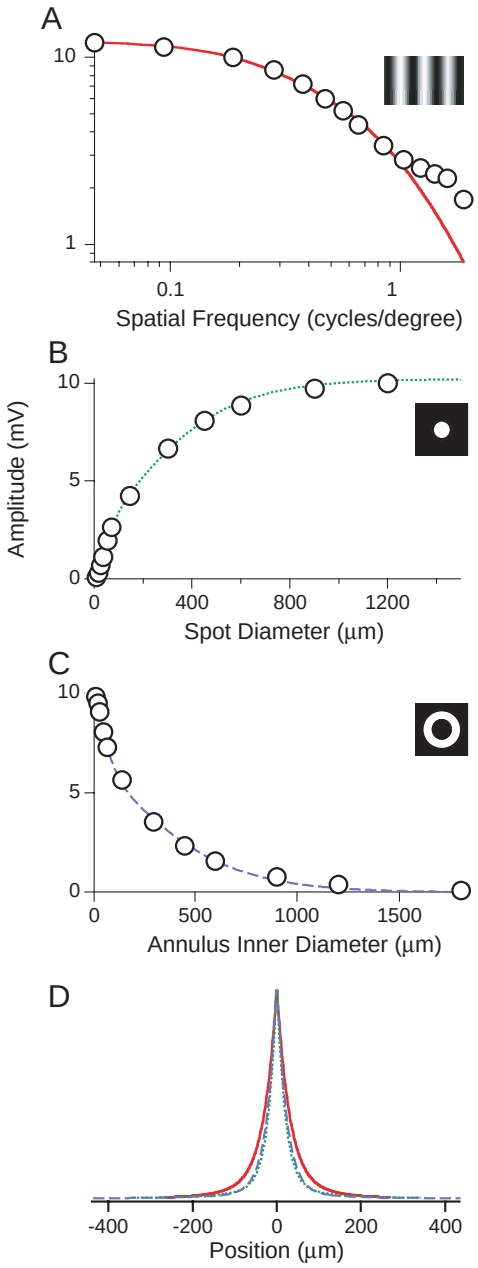

Figure 2. Receptive fields measured in a single cell with gratings, spots, and annuli. The open circles are data points. The solid (red), dotted (green), and dashed (blue) curves represent the sum of two exponentials' fits to grating, spot, and annular stimuli, respectively. a. Spatial tuning curve measured with drifting sine wave gratings. Fundamental amplitude in millivolts is plotted as a function of spatial frequency in cycles/degree. b. Area summation curve measured with flashing spots. Amplitude in millivolts is plotted as a function of spot diameter in μm. c. Annulus summation curve measured with flashing annuli. Amplitude in millivolts is plotted as a function of the inner annulus diameter in μm. d. Receptive field profiles derived from responses to all three stimuli. Each plot shows response amplitude in arbitrary units as a function of radial distance in μm from the center of the receptive field.

for the three possible stimulus pairings. The grating/spot, spot/annulus, and annulus/grating diameter ratios were 0.87 ± 0.43, 1.17 ± 0.77, and 1.58 ± 1.34, respectively. None of the three ratios differed significantly from 1. Because the responses to the three stimulus types produced similar estimates of receptive field size and shape, we made most of our measurements using gratings.

H1 receptive field structure

H1 cells responded to drifting sine wave gratings with a sinusoidal voltage modulation (Figure 3). At low spatial frequencies (Figure 3, top curves), the response faithfully followed the modulation of the stimulus. As spatial frequency increased, response amplitude decreased. The response amplitudes of some cells declined smoothly as spatial frequency increased (Figure 3, Cell 1), whereas the amplitudes of other cells decreased nonmonotonically (Figure 3, Cell 6). The response to sinusoidal modulation was free of gross low frequency harmonic distortion at all spatial frequencies that elicited a strong response. Less obvious distortions, such as an asymmetry in the shapes of the response peak and the response minimum, were similar to those previously reported (Smith et al., 2001).

Spatial tuning curves (Figure 4, open circles) spanned a continuous range of shapes from smoothly low pass (Figure 4, top) to prominently notched (Figure 4, bottom). The response amplitude of the large majority of cells (n = 125 of 158, 79%) decreased monotonically with increasing spatial frequency. Some responses decreased smoothly with increasing spatial frequency (Figure 4, top) whereas others had a slight inflection or a more pronounced shoulder (Figure 4,middle). Even those cells with the smoothest tuning curves had more power at high spatial frequencies than a single exponential could account for. However, these cells could be well described by a sum of two exponentials (Figures 4, top, black curves). Often there was more power at the highest spatial frequencies than could be strictly accounted for by even a sum of exponentials. This energy took the form of a slight upward inflection of the data points at high spatial frequencies, but was rarely large enough to seriously degrade the fit.

The tuning curves of the remaining cells (n = 33, 21%) were more complex than the simple low pass shape expected of a cell that simply sums signals from L and M cones. These tuning curves had one or more high amplitude peaks at moderate to high spatial frequencies (Figure 4, bottom 2 curves). These additional peaks occurred at similar spatial frequencies for each measurement of a single cell, but varied in position from cell to cell. They were also well above the noise level of the recording. We will consider possible explanations for these peaks in the "Discussion."

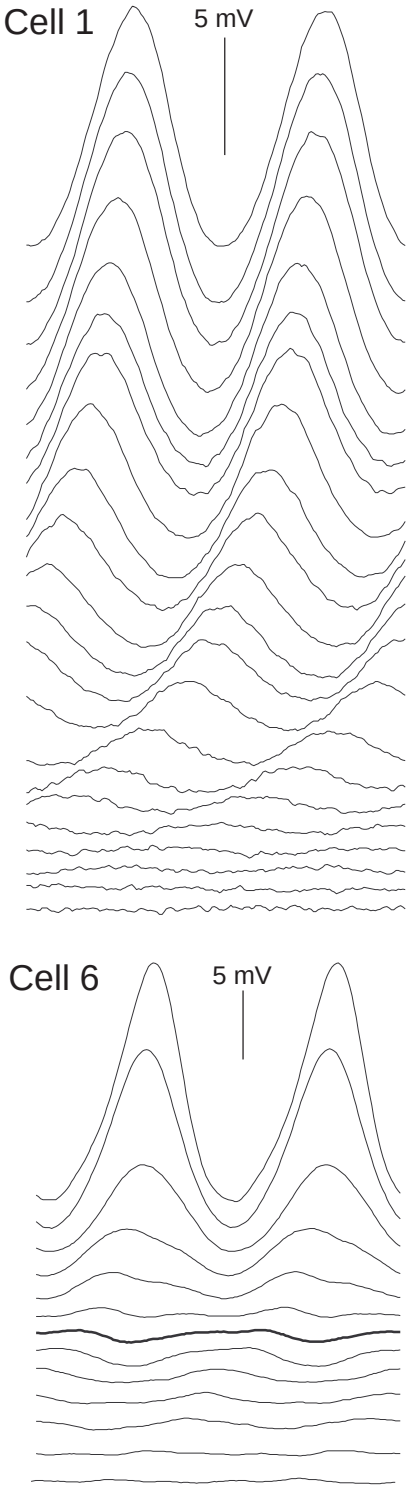

Figure 3. Examples of H1 cell responses to drifting sine wave gratings. Each trace is two cycles of the averaged response to a drifting grating of a particular spatial frequency. Spatial frequency increases from top to bottom. The scale bar indicates response amplitude. Cell 1 had a spatial tuning curve that rolled off smoothly as a function of eccentricity (Figure 4, top curve). Cell 6 had a tuning curve with a large notch (thick curve) and peak at intermediate spatial frequencies (Figure 4, bottom curve).

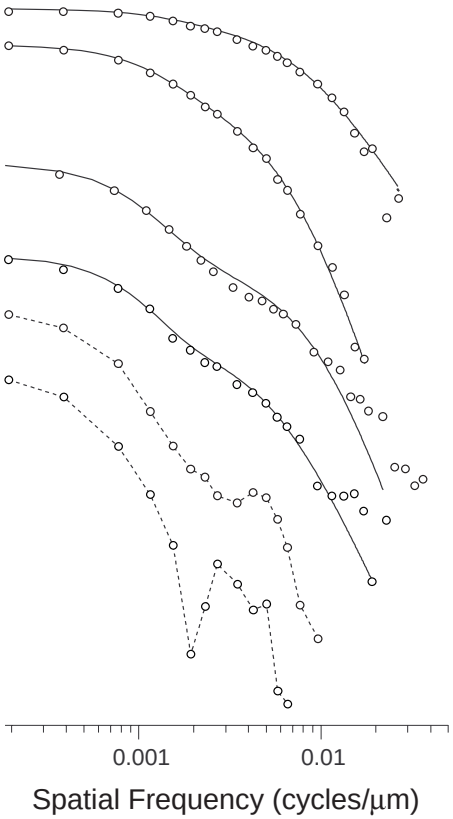

Figure 4. Examples of the diverse shapes of H1 spatial tuning curves. Each graph plots the fundamental response amplitude (open circles) in arbitrary units as a function of the spatial frequency in cycles/μm of a drifting sine wave grating. The solid black line in each of the top 4 curves is the best fitting sums of exponentials. The dashed black line in the bottom 2 curves simply connects the data points. The top curve is Cell 1. The bottom curve is Cell 6.

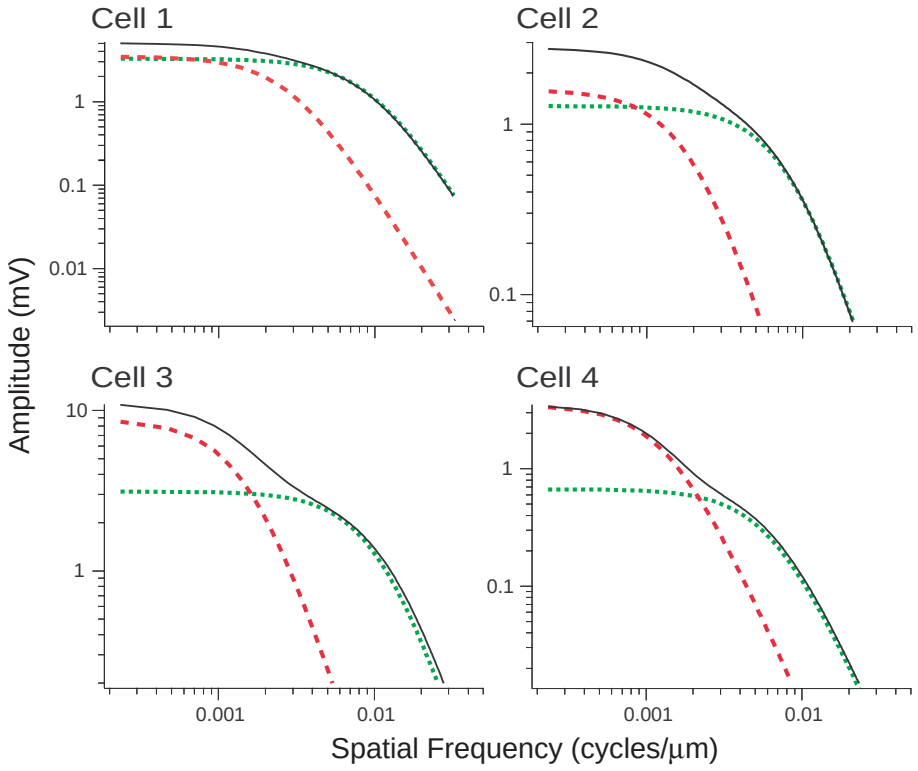

Figure 5. Sum of exponential fits to the top four spatial tuning curves of Figure 4. The black line is the best fitting sum of exponentials. The green dotted and red dashed curves are the component exponentials. Note that the two exponentials do not always add precisely to the sum because phase is taken into account and the phases of the two components were not always identical. To facilitate the comparison of shape, all graphs were plotted on axes of the same physical lengths. This is equivalent to normalizing the responses to maximum amplitude.

Each sum of exponentials fit (Figure 4, top 4 curves) can be thought of in terms of two separate exponential components (Figure 5), one that rolls off at a lower spatial frequency and one that rolls off at a higher spatial frequency. When the two components were of similar amplitude (Figure 5, Cells 1 and 2), their sum (black curve) rolled off smoothly. When the two components were of quite different amplitude (Figure 5, Cells 3 and 4), their sum had a distinct shoulder.

The receptive field sensitivity profile of most H1 cells (Figure 6, black curves) took the form of a prominent central peak (green dotted curve, hereafter called the narrow field) superimposed on a broad shallow skirt (red dashed curve, hereafter called the wide field). This was most easily seen by looking directly at receptive field profiles. The receptive field profiles for the cells whose spatial tuning curves were illustrated in Figure 5 were calculated from the Fourier transforms of the best fitting sum of exponentials. Every cell had a substantial contribution from both the narrow and wide fields, but their widths and heights varied considerably. Even in this small set of examples (Figure 6), there was a factor of two range of diameters for the narrow (115 to 221 μm), wide (515 to 1035 μm), and summed fields (133 to 299 μm). The relative weights of the narrow and wide fields (the ratio of the volumes of their receptive fields) varied over a factor of 5 (1 to 0.2). The volume of the wide field was often similar to that of the narrow field not because wide field sensitivity was high at any given location but because of its larger lateral extent. In this respect, it was much like the surround in a center/surround receptive field.

A second way of seeing that most of the sensitivity near the center of the receptive field was mediated by the narrow field was to compare the diameters of the narrow and summed receptive fields (Figure 7). We will come back to the full significance of this figure in the next section. For the moment, note that each cell was represented by two symbols plotted at the cell's eccentricity, one (open circle) representing the diameter of the summed field and the other (solid black circle) representing the diameter of the narrow field. If the summed field was dominated by the narrow field, then the diameter of the summed field would be only modestly greater than that of the narrow field. This was true of most cells.

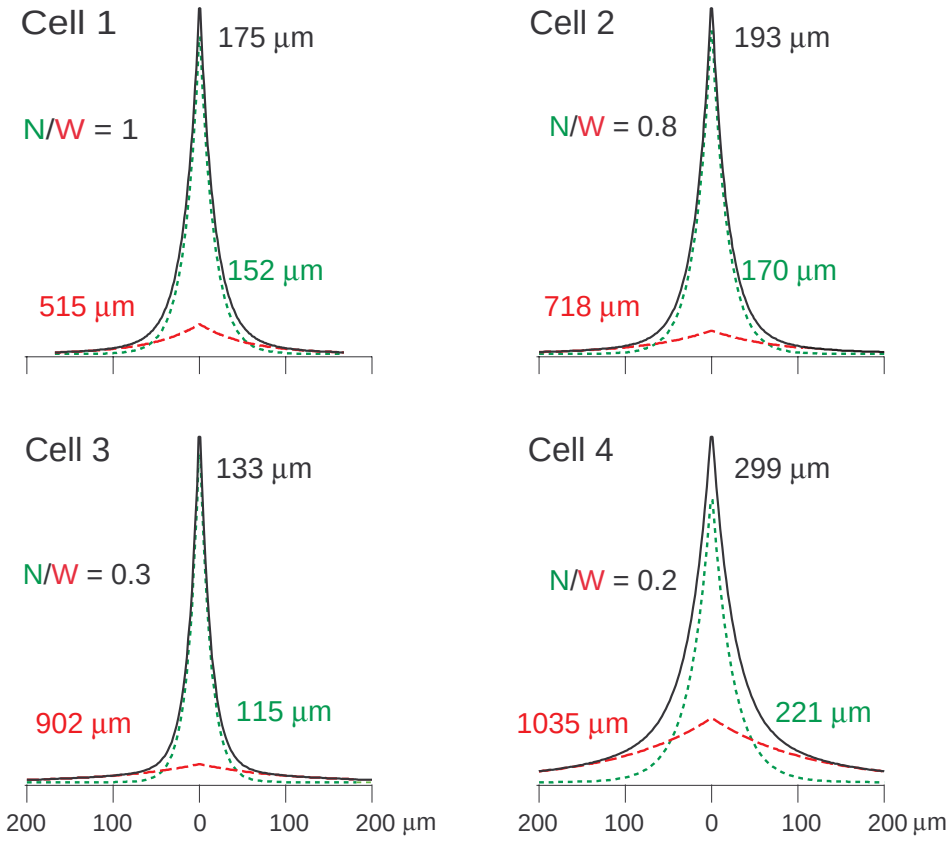

Figure 6. The receptive field sensitivity profiles of the cells shown in Figure 5. Each graph plots sensitivity in arbitrary units as a function of radial distance in μm from the receptive field center. Each curve was calculated from the Fourier transform of the spatial tuning curve shown in Figure 5. The black curve is the best fitting sum of exponentials. The wide (red dashed) and narrow (green dotted) curves are the exponential components. The color-coded numbers are receptive field diameters measured at 0.1 of peak amplitude.

Receptive field diameter increases with increasing eccentricity

The average receptive field diameter of H1 cells, evaluated by fitting an exponential through the cloud of measurements, increased with increasing eccentricity from 122 μm at 4 mm of eccentricity to 309 μm at 11 mm of eccentricity (Figure 7, black curve). However, the upward trend in receptive field size as a function of eccentricity appeared to be due to the increasing number and size of the larger receptive fields rather than to a general increase in the receptive field size of all cells. Substantial numbers of cells (Figure 7, open circles) at all eccentricities had small receptive fields less than 200 μm in diameter. At eccentricities greater than 6 mm, an increasing number of cells had much larger receptive fields. It was these cells that raised the average receptive field diameter at larger eccentricities. At any eccentricity at which many receptive fields were measured, the range of diameters was more or less continuous.

The smaller receptive fields had diameters similar to those of dendritic trees at all eccentricities, whereas the largest receptive fields were much larger than any dendritic arbor. This was seen by comparing dendritic tree diameters measured from Golgi stained retinas (Wässle et al., 1989) to our receptive field measurements. Receptive field diameter estimated from the exponential fit (Figure 7, black curve) was about twice that of average dendritic tree diameter (Figure 7, gray area) at any given eccentricity. Wässle et al. (1989) measured dendritic area by tracing around the individual dendrites, keeping far enough from them to include the cone contacts. Had the measurement been based on the area of a convex polygon enclosing the tips of the dendrites, the anatomical diameters would be larger.

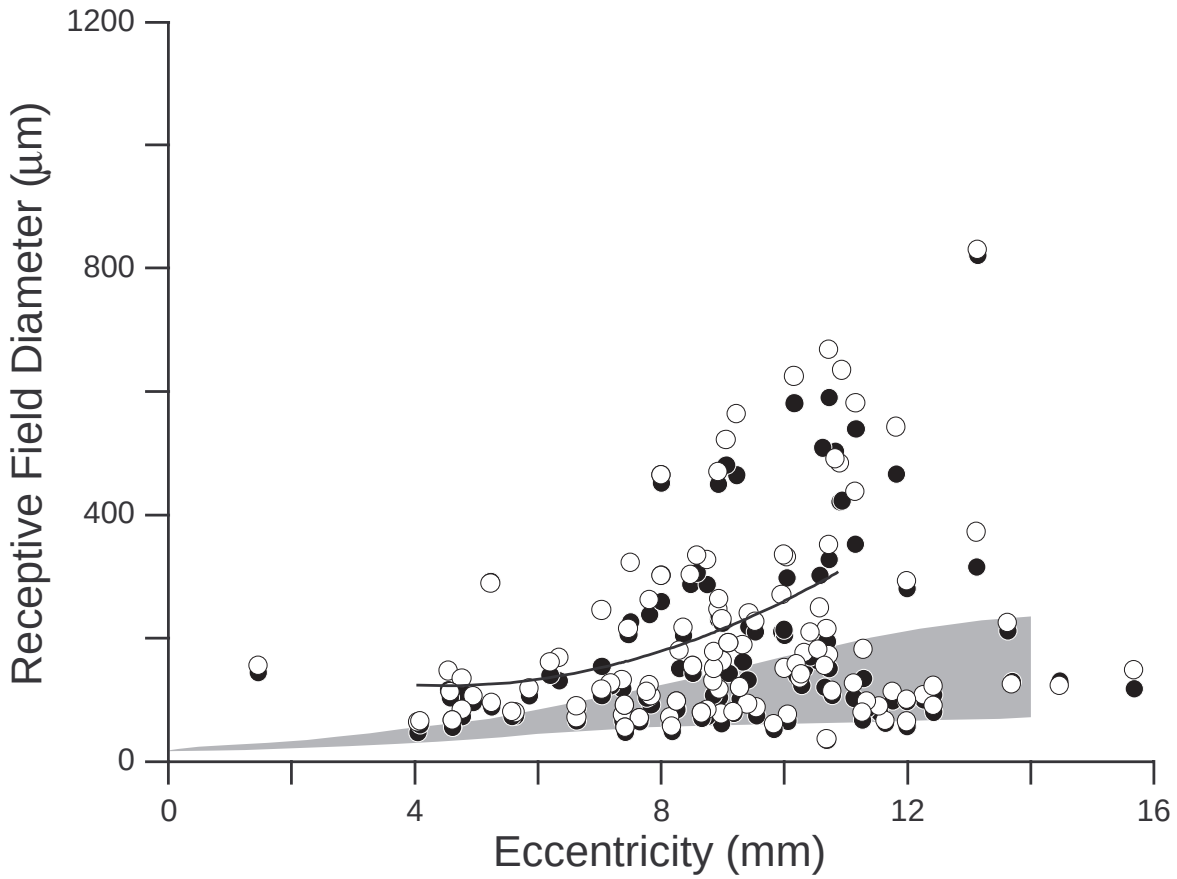

Figure 7. Receptive field diameter plotted as a function of eccentricity. Receptive field diameter in μm was calculated by fitting a sum of two exponentials to spatial tuning curves (n = 125) measured using drifting sine wave gratings. Those cells located in temporal, superior, and inferior retina were plotted at their physical eccentricities. Those cells in nasal retina were plotted at their temporal equivalent eccentricities (Watanabe & Rodieck, 1989). Each open circle is the diameter of the sum of the narrow and wide fields of the receptive field. The black line is the exponential fit ($y = y_0 + A\exp(-tx)$, $y_0 = 116.15$, $A = 0.01857$, $t = 3.8718$) to the summed field. The fit was made with data up to 11 mm of eccentricity because at greater eccentricities the number of cells measured was too small to capture the full range of receptive field sizes. Each solid black circle is the diameter of the narrow field. The gray area encloses the dendritic tree diameters calculated from dendritic tree area (Wässle et al., 1989). Receptive field diameter was measured at 0.1 of peak value.

Comparing the receptive fields and the dendritic trees of individual cells

The simplest explanation for the two-component receptive field structure is that the narrow field corresponds to direct synaptic input from the cones overlying the dendrites and the wide field corresponds to coupled input from neighboring H1 cells. If so, the diameter of the receptive field and the dendritic tree should be similar in cells with weak coupling whereas those cells with stronger coupling should have receptive fields that are larger than their dendritic fields. To see if this relationship held in primate retina, we compared directly the receptive fields and dendritic arbors of 19 H1 cells that were filled intracellularly with biocytin-X-hydrazide (Figure 8).

The range of H1 morphology across the retina (Wässle et al., 1989) correlated with receptive field physiology and is probably related to variations in coupling strength. At all eccentricities, there is a population of cells with small receptive fields (Figure 7). These cells tend to have dendrites that are short, but extensively branched (Figure 8, lower left). The similar size of receptive fields and dendritic trees suggests that these cells are weakly coupled, probably due to lack of overlap with neighboring dendritic trees. At greater eccentricities, cells with a range of larger receptive fields become common. These cells have dendritic trees that are smaller than their receptive fields. Morphologically, the dendrites of these cells tend to be sparse and less extensively branched (Figure 8, lower right). The large receptive and smaller dendritic fields of these cells suggest that they are more strongly coupled probably due to greater overlap with neighboring dendritic trees. These examples represent the morphological extremes, but except in central retina where cells with small receptive fields predominate, there is a more or less continuous range of receptive field sizes and dendritic morphologies (Figure 8, graph).

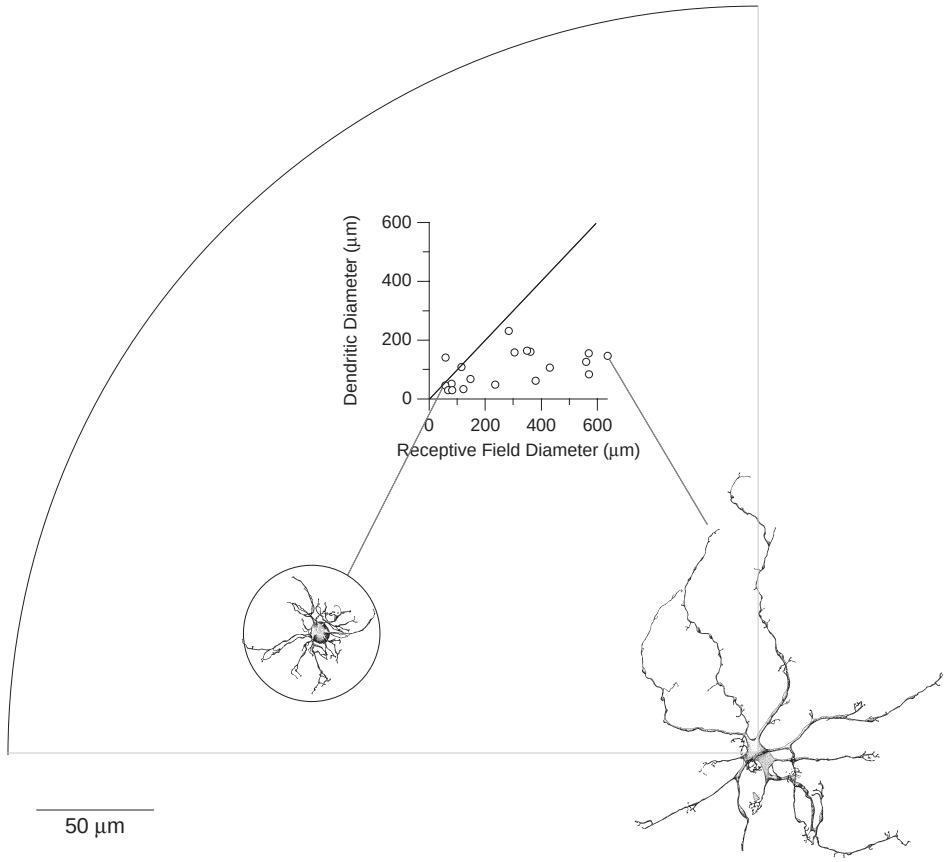

Figure 8. The relationship between the receptive fields and dendritic trees of 19 H1 horizontal cells. Each cell (open circle) is represented by plotting the diameter in μm of the dendritic tree as a function of the diameter of the summed receptive field. The diagonal line represents equal dendritic and receptive field diameters. The dendritic trees of two cells indicated by the gray lines between cell and graph have been drawn to scale. Around each drawing is a circle (small cell) or an arc (large cell) representing the receptive field of that cell. The small cell had receptive field and dendritic diameters of 58 and 45 μm, respectively. The large cell had receptive field and dendritic diameters of 637 and 146 μm, respectively. The scale bar indicates distance in μm.

Other Properties of the Receptive Field

Our conclusions about the spatial properties of H1 cell receptive fields depend on certain assumptions about the response of the H1 cell to light. We assumed that the receptive field of the H1 cell was circularly symmetric, that the cell responded to light and contrast in a linear way, that the organization of the H1 receptive fields did not depend on light level, and that the cells were summing inputs from L and M cones only.

Response linearity to drifting gratings

The linear component of the response of monkey H1 cells to drifting gratings accounted for nearly all of the response over the range of spatial and temporal frequencies used in these experiments. When stimulated with a drifting grating, and allowing for a delay in response onset, the response of H1 cells closely followed stimulus amplitude. This was true at temporal frequencies between 1 and 10 Hz and at spatial frequencies up to at least 0.01 cycles/μm (2 cycles/degree). Nearly all of the amplitude in the temporal frequency spectrum of a drifting grating occurred at the drift frequency. When the temporal response was decomposed using Fourier analysis, the amplitude of the harmonic component at twice the drift frequency was seldom greater than 1% of the amplitude at the drift frequency. Higher harmonics had even less amplitude. H1 horizontal cells respond to spots and annuli in a similar way (Dacey et al., 1996; Smith et al., 2001), as do cat horizontal cells (Lankheet, Prickaerts, & van de Grind, 1992).

Contrast response linearity

Response amplitude scaled linearly with stimulus contrast. We measured responses using as much contrast as possible under conditions that stimulated the cell weakly. This risks saturating the response. We measured the spatial tuning curves of 35 cells over a range of grating contrasts between 5% and 100%. Four cells were measured at 5 different contrasts (Figure 9). The amplitude of each tuning curve was scaled by the inverse of grating contrast. After rescaling, the spatial tuning curves superimposed. In particular, there was no evidence that 100% contrast gratings were saturating the response. Lastly, the tuning curves of cells with additional peaks (Figure 9, Cells 1, 2, and 4) looked similar at all contrasts, suggesting that peak location was not affected by stimulus contrast.

Receptive field symmetry

The irregularity in both length and angle with which H1 dendrites radiate (Wässle et al., 1989) could be manifest physiologically in the form of asymmetric receptive fields. A drifting grating is an excellent stimulus for measuring receptive field symmetry because it measures a one-dimensional slice of the two-dimensional spatial tuning surface.

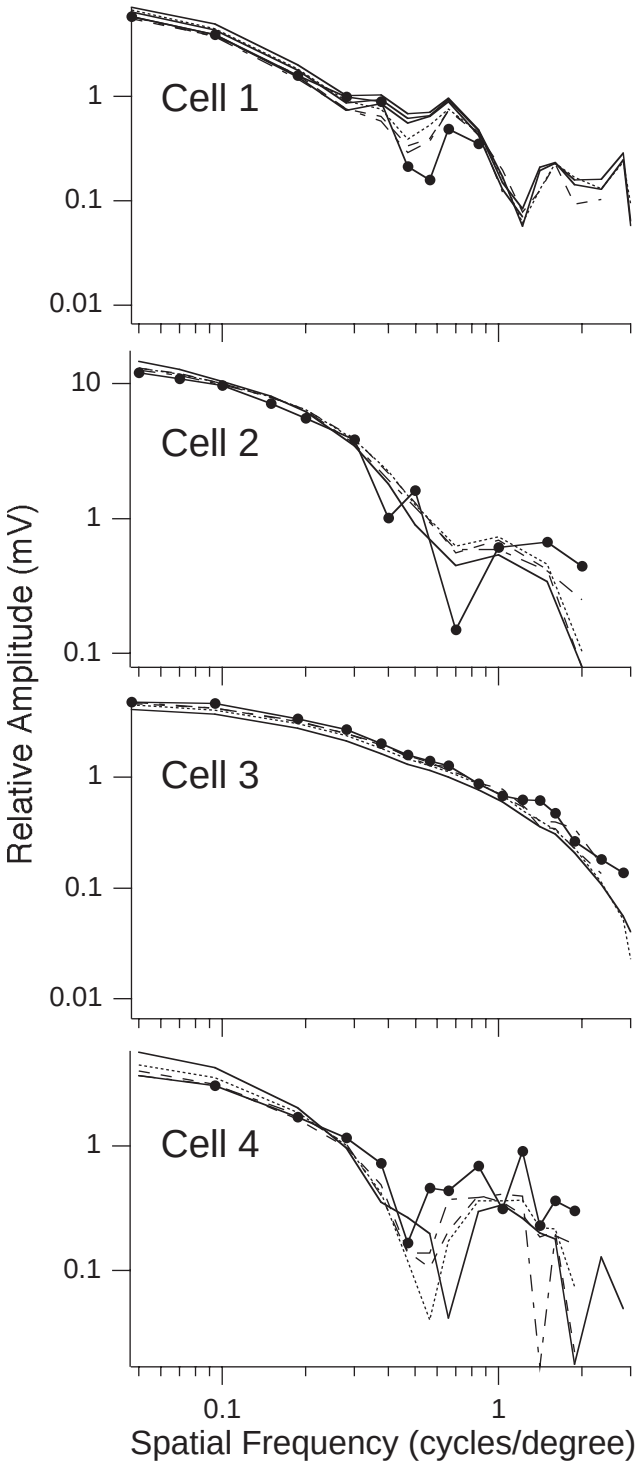

Figure 9. Modulation transfer as a function of grating contrast for 4 H1 horizontal cells. Each plot shows a series of spatial tuning curves collected across a range of contrasts (5,10,25,50, and 100%). Each curve is the fundamental response of the cell in millivolts to a range of spatial frequencies measured in cycles/degree. The responses were normalized by scaling them by the inverse of stimulus contrast. (e.g., 5% contrast is scaled by 1/0.05 = 20). The solid lines, lines with dots, dashed lines, dot-dash lines, and dotted lines represent 5, 10, 25, 50, and 100% contrasts, respectively.

Surprisingly perhaps, in light of their dendritic anatomy, H1 cells had nearly circular receptive fields. Spatial tuning curves were measured in 8 cells using grating orientations of 0, 45, 90, and 135 degrees. Four of those cells are shown in Figure 10. Each plot shows data from a single cell and each curve represents a single grating orientation. At lower spatial frequencies, all orientations produced identical responses. The curves diverged somewhat above 0.4 cycles/degree, but there was no systematic ordering that suggested an asymmetry common to all of the receptive fields in an area. Further, in 2 cells (Figure 10, Cells 2 and 3), a repeated measure at the 0 degree orientation was as variable as measurements across orientation. Differences in shape that might be introduced by asymmetries in the dendritic fields were apparently averaged out, probably by coupling. As a result, the receptive field of an H1 horizontal cell can be characterized by a spatial tuning curve measured at a single grating orientation. Orientation also had no dramatic effect on the positions or height of additional peaks (Figure 10, Cells 1 and 2), although there was some variability.

Effect of light level on receptive field size

In nonmammalian retina, the size of horizontal cell receptive fields decreases as light level increases (Yamada, Yasui, Furukawa, Petruv, & Djamgoz, 1995; Pottek & Weiler, 2000). This change is thought to result from a change in coupling mediated by gap junction modulators (Piccolino, Neyton, & Gerschenfeld, 1984; Tornqvist et al., 1988) whose release depends on the level of light adaptation (Kirsch & Wagner, 1989). No similar effect has been demonstrated in mammalian retina. Previous measurements made in our laboratory (Verweij, Dacey, Peterson, & Buck, 1999) showed no change in receptive field size when a dark adapted H1 cell was illuminated by a slit that was either bright red to stimulate cones or dim blue to stimulate rods.

At the light levels used in these experiments, we found no evidence for changes in receptive field size. The adaptational state of the retina was held constant by modulating the stimulus around a mean level of ~1,000 trolands. The retina saw the same space and time averaged luminance whether or not the stimulus was present. To control for the possibility that light level might be affecting the spatial characteristics of the receptive field, we measured the spatial tuning curves of 6 cells at two or more light levels ranging from 10 to 10,000 trolands. Before each measurement, the cell adapted for 15 min to the mean light level of the stimulus. Two examples of receptive field sensitivity as a function of light level are shown in Figure 11. Both cells were measured at 10, 100, and 1,000 trolands. None of the 6 cells showed a systematic change in receptive field size as a function of light level.

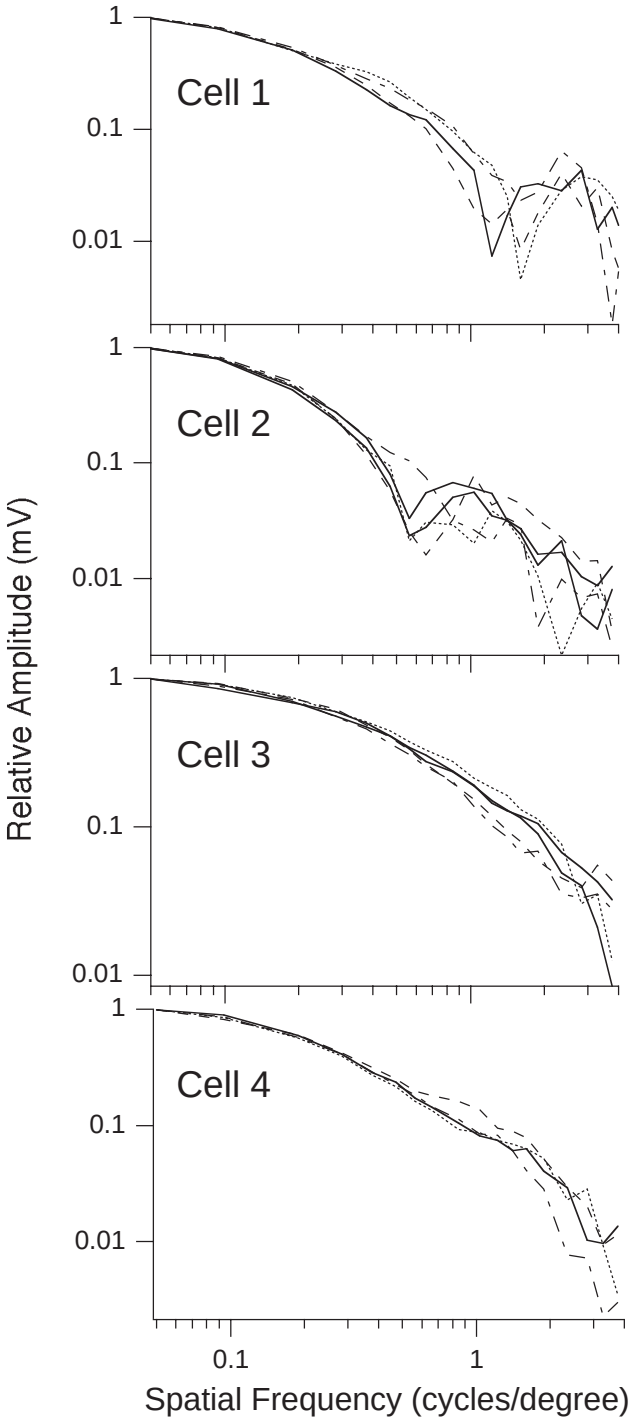

Figure 10. The effect of grating orientation on the spatial tuning of 4 H1 cells. Each plot shows a series of spatial tuning curves collected with 100% contrast gratings rotated in intervals of 45 degrees. Each curve is the fundamental response in millivolts across a range of spatial frequencies measured in cycles/degree. The solid, dashed, dot-dashed, and dotted curves represent orientations of 0, 45, 90, and 135 degrees, respectively. For a grating orientation of 0 degrees, the bars of the grating were perpendicular to the horizontal meridian of the retina. Higher orientations represent clockwise rotation around the fovea.

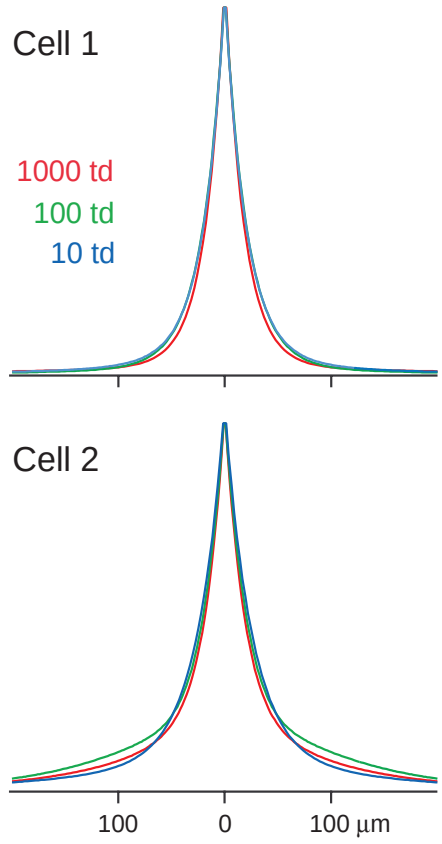

Figure 11. Receptive field sensitivity profiles from 2 H1 cells calculated from spatial tuning curves measured at light levels of 1,000 (red), 100 (green), and 10 (blue) trolands, respectively. The x axis is position in µm relative to the center of the receptive field. The y axis is arbitrary, but all three light levels used the same scale.

Cone inputs to the receptive field

We measured the chromatic properties of the cone inputs to the majority of cells using two stimuli. The first stimulus provided a quick estimate of the relative strengths of the L, M, and S cone inputs by measuring the response of each cone type in isolation. Every cell that was tested responded strongly to L and M cone stimulation but negligibly to S cone stimulation. The second stimulus held the mean photon catch for each cone type constant while varying the strength of L and M cone input over a range from pure L to pure M cone input. L and M cone stimulation was of opposite phase causing the response of the cell to be minimized at the L/M input ratio of the cell. The results were nearly identical to those already reported (Dacey et al., 1996; Dacey, Diller, et al., 2000), namely, that the ratio of L and M cone inputs varied widely around a mean L/(L+M) ratio of ~0.6. These data confirm that the measurements of relative cone input made with the digital light projector-based stimulator are similar to previous measurements made using a light emitting diode–based stimulator.

Discussion

H1 Receptive Field Organization

We have suggested that the tall narrow peak of the H1 receptive field reflects direct synaptic input from cones, whereas the broad shallow skirt reflects coupled inputs from neighboring H1 cells. However, the two-component receptive field might simply reflect the geometric and synaptic properties of dendrites. The long distal dendrites get fewer cone inputs and have fewer opportunities to form gap junctions (Figure 8). Because they are thin, they may have high internal electrical resistance that reduces the effectiveness of the contacts that they do make (Rall, 1959). The proximal dendritic trees of these cells tended to be more extensively branched, making more cone contacts and providing more potential sites for gap junctions between short, wide sections of proximal dendrite that have low electrical resistance. Thus the narrow receptive field might be mediated by those cone contacts and gap junctions close enough to effectively drive the cell while the wide field might be composed of sparser cone contacts and gap junctions so far away that their effectiveness is reduced to that of a broad background. This hypothesis does not explain, however, why the narrow and wide components are so distinct.

Like other foveal neurons, H1 cells have very small receptive fields and dendritic trees. H1 foveal anatomy features high cell density (5 times that of far periphery, Wässle et al., 2000) and small barely overlapping dendritic trees (as small as 20 µm, Figure 12, left). Central receptive fields were similar in diameter to their dendritic trees. A decreased opportunity for coupling is likely the reason for the similarity in receptive field and dendritic diameters. We measured only a few H1 receptive fields at eccentricities less than 4 mm. However, this lack of coupling suggests that central receptive fields may be as small as central dendritic trees. If so, a foveal H1 cell that gets input primarily from the 6 or 7 cones contacted by its dendritic tree (Wässle et al., 1989) will have the small weakly coupled receptive field required for generating surrounds in the midget cell pathway. In peripheral retina, H1 cells had a range of morphologies (Wässle et al., 1989) and these differences were reflected physiologically. The dendritic fields of large peripheral H1 cells had long sparsely branched dendrites that contacted as many as 50 cones. Other cells had small extensively branched dendritic trees that contacted only a half dozen cones (Figure 1). In between these extremes were a range of dendritic diameters. The physiological receptive fields of H1 cells were similarly variable. Mean receptive field diameter was 309 µm at 11 mm of eccentricity, but some receptive fields were more than twice as large, whereas others were 5 times smaller. Those

cells that had smaller dendritic trees tended to have smaller receptive fields and vice versa. In spite of these differences in anatomy and physiology, these cells always sum L and M cone inputs exclusively and form a single coupled population with variable dendritic and receptive field diameters. A closer look at the functional significance of these individual differences between cells will require modeling the network properties of an H1 mosaic with a similar range of properties.

The multiple peaks in the spatial tuning curves of ~20% of the cells at moderate to high spatial frequencies are likely due to undersampling of the retinal image by H1 circuitry. When too few cells sample the image, high spatial frequencies are misinterpreted as lower spatial frequencies (Shannon, 1949), potentially forming additional peaks in the spatial tuning curve. This phenomenon, known as aliasing, has been extensively documented in the photoreceptor mosaic (Williams, 1985; Williams, 1988; Thibos, 2000) but is theoretically possible in any coupled network. The location and height of these peaks would depend in a complex way on the locations of cones and H1 cells in their mosaics as well as the diameters of their receptive fields. Because these parameters are unknown, the existence of multiple peaks is consistent with but not definitive proof of aliasing. If the peaks were due to aliasing by the H1 network they should disappear if the network was uncoupled. Experiments using the gap junction blocker carbenoxolone show that this does occur (Packer & Dacey, 2001). A less likely alternative is that the peaks represent receptive field subunits, small regions of high sensitivity outside the classic receptive field. In ganglion cells, it has been suggested that subunits are caused by complex irregularities in ganglion cell dendritic sampling of bipolar inputs (Hochstein & Shapley, 1976; Thibos & Levick, 1983; Kaplan & Shapley, 1982; Soodak, Shapley, & Kaplan, 1991) or by long distance inputs from outside the classic receptive field (Taylor, 1999; Demb et al., 1999). If the additional peaks were due to analogous asymmetries in the H1 dendritic tree or in gap junction connectivity, peak height and location would change with grating orientation. Because they do not, the additional peaks are probably not subunits.

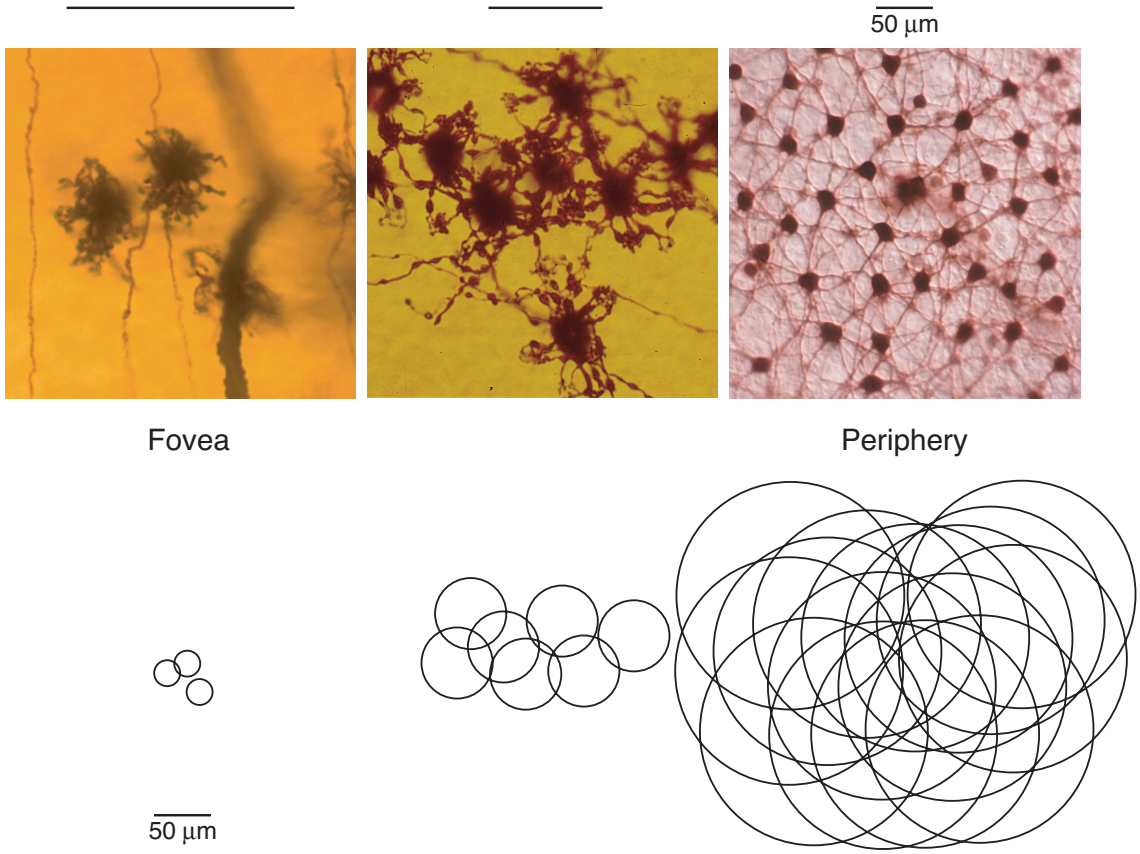

Figure 12. A summary of H1 anatomy and receptive field size in macaque retina. Top row. Images of H1 horizontal cells in the central fovea (left), on the foveal slope (center), and in far periphery (right). The two images on the left are of Golgi stained H1 cells. In the right image, a single H1 cell was filled with biocytin and reacted using standard horseradish-peroxidase histochemistry. The scale bar above each image represents 50 μm. Bottom row. Each circle represents an H1 receptive field whose center location was digitized from the image in the top row. The diameter of each circle represents mean receptive field diameter at that location. The scale bar indicates 50 μm at all three eccentricities.

A Comparison of Vertebrate Horizontal Cell Networks

The anatomy of the macaque H1 network is similar in fundamental ways to the horizontal cell networks of other vertebrates (Naka & Rushton, 1967; Lamb, 1976; Lankheet et al., 1992) but also has important differences. Like the horizontal cells of other vertebrates, H1 dendritic trees contact cones, overlap each other, and are coupled by gap junctions. The most striking difference between the primate horizontal cell network and that of other vertebrates is the degree to which the presence of the fovea is reflected in the form of higher cell density, smaller dendritic trees, and lower dendritic overlap. The cat retina also has a central region of higher photoreceptor density, the area centralis, but horizontal cell morphology does not reflect the same degree of specialization found in the primate fovea.

The physiology of the macaque H1 network is also similar in certain fundamental ways to the horizontal cell network of other vertebrates. The spatially nonopponent nature of H1 receptive fields, the linearity of spatial summation, and the spatio-temporal separability of the receptive field at lower temporal frequencies are common to all vertebrates. Unlike other vertebrates, the macaque H1 network is less strongly coupled, has smaller receptive fields, and shows no functional plasticity. Taken together these differences profoundly affect how the H1 network functions. Macaque H1 receptive fields are poorly fit by the infinite sheet model (Naka & Rushton, 1967), which is based on a passive horizontal cell network in which direct synaptic input is swamped by coupled input. The opposite is true of macaque H1 cells whose central receptive fields get only a small percentage of their total response from the coupled field. The uniformly large receptive fields of cat horizontal cells suggest more extensive coupling than that found in macaque retina. This may account for some differences between cat and monkey horizontal cell physiology. For example, the line weighting function estimated the cat horizontal cell receptive field to be several times larger than the estimate derived from the spatial tuning curve measured with gratings (Lankheet, Frens, & van de Grind, 1990; Lankeet et al., 1992). Our estimates of receptive field size in macaque H1 cells were similar regardless of stimulus configuration. Lastly, we found no evidence that receptive field size in the macaque horizontal cell network depends on light level as it does in some nonmammalian retinas (Yamada et al., 1995; Pottek & Weiler, 2000), suggesting that, at least over the range of light levels that we use in experiments, there is no functional reorganization that trades resolution for light-gathering ability under low-light conditions.

Perhaps the most striking difference between the primate horizontal cell network and that of other vertebrates is the degree to which the presence of the fovea is reflected in the physiology. In cat retina, increased cell density has not been correlated with a reduction in horizontal cell receptive field size as a function of decreasing retinal eccentricity (Lankheet et al., 1990, 1992; Nelson, 1977), a correlation that is very strong in primate retina. This probably reflects the large central receptive fields and shallower peripheral to central density gradient found in the cat horizontal cell network. As a result, eccentricity related changes in the properties of cat horizontal cells would be weaker and thus harder to measure.

A strong correlation between tracer coupling and functional coupling is not a feature of the macaque H1 cell network. It is tempting to assume that tracer coupling between H1 cells correlates with functional enlargement of the H1 receptive field, although there are many differences in the mechanisms by which ions and biocytin cross gap junctions (Mills & Massey, 1998). In most vertebrates, horizontal cell tracer coupling is extensive and receptive fields are larger than dendritic fields (cf., Tomita, 1965; Naka & Rushton, 1967; Naka & Witkovsky, 1972; Mangel, 1991; Bloomfield et al., 1995). However, the degree to which coupling is related to receptive field size varies. In the amacrine cells of lower vertebrates, receptive fields are larger than dendritic fields (Hidaka, Maehara, Umino, Lu, & Hashimoto, 1993; Teranishi & Negishi, 1994). On the other hand, the receptive and dendritic fields of mammalian amacrine and ganglion cells can be quite similar in size (Peichl & Wässle, 1983; Bloomfield, 1992; Yang & Masland, 1994; Taylor & Wässle, 1995; Peters & Masland, 1996; Taylor, 1996; Stafford & Dacey, 1997) in spite of the fact that tracer coupling reveals entire mosaics of these cells (Vaney, 1994; Stafford & Dacey, 1997). In the rabbit horizontal cell network, the extent of biocytin spread is reported to be related closely to functional coupling (Bloomfield et al., 1995). In macaque, the spread of biocytin dramatically overestimates H1 receptive field size. Tracer coupling (Dacey et al., 1996; Wässle et al., 2000) extends to cells >1 mm away from the filled cell, whereas average receptive field diameter is only ~300 μm even at 11 mm of eccentricity.

Implications for Center/Surround Organization

Decreases in both dendritic field diameter and dendritic tree overlap from periphery to fovea probably reduce H1 receptive field diameter sufficiently to allow H1 cells to form the surrounds of ganglion cells across the retina. Peripheral H1 receptive fields are clearly smaller than the surrounds of either bipolar or ganglion cells. A group of 5 parasol and 7 midget ganglion cells had mean surround diameters of 1,014 and 856 μm, respectively, whereas a group of 8 diffuse and 4 midget bipolar cells had surround diameters of 743 and 467μm, respectively (Dacey, Packer, et al., 2000). Similarly, Croner and Kaplan (1995) reported that ganglion cell surrounds are

~500 μm in diameter at an eccentricity of 8 mm. In contrast, the H1 receptive fields (Figure 7) had mean diameters of 309 μm at 11 mm of eccentricity. In the fovea, the smallest surrounds are those of the midget ganglion cells. These midget cells have receptive field surround diameters between 20 and 30 μm (Lee et al., 1998; Croner & Kaplan, 1995). At all eccentricities between 4 and 12 mm, we recorded substantial numbers of cells with receptive field diameters less than 100 μm and as small as 42 μm (Figure 7). The downward trend in receptive field size as eccentricity decreases together with the limited coupling measured physiologically suggests that the most central H1 cells likely have receptive field diameters as small as those of central midget surrounds.

These H1 receptive field measurements are consistent with a range of evidence that H1 horizontal cells mediate the inhibitory surrounds of macaque midget cells. Even so, there have been recent suggestions that amacrine cells also play a role in surround formation (Flores-Herr, Protti, & Wässle, 2001; Bloomfield & Xin, 2000; Euler & Masland, 2000; Taylor, 1999; Demb et al., 1999). Recent experiments show that the gap junction blocker carbenoxolone (Packer & Dacey, 2001) eliminates the small, slow depolarization that occurs after an H1 cell hyperpolarizes to light. This effect, which is thought to be the result of feedback from H1 cells onto cones (Kamermans et al., 2001), is consistent with the hypothesis that carbenoxolone blocks H1 feedback onto cones. Preliminary evidence from our laboratory also shows that carbenoxolone selectively eliminates the surround of parasol ganglion cells, suggesting that feedback from H1 cells to cones is the primary contributor to inhibitory surrounds.

Implications for Color-Opponent Models of the Midget Pathway

Red/green spectral opponency results when a midget cell receptive field center gets input from either an L or M cone while the surround gets input from the opposite cone type. The "selective connection" hypothesis requires cone specific circuitry to conduct signals from the cone type opposite that of the center to the surround. Measurements of the chromatic inputs to midget ganglion cell surrounds (Reid & Shapley, 1992; Lankheet, Lennie, & Krauskopf, 1998; Lee et al., 1998; Smith, Lee, Pokorny, Martin, & Valberg, 1992) disagree about the purity of surround input. However, if surrounds are pure, a selective mechanism must channel pure cone input to the surround. H1 cells are the only outer retina cell type with the required lateral connections but they sum L and M cone input (Dacey et al., 1996). The amacrine cells of inner retina are the other candidate for making selective lateral connections, but they also get indiscriminate input from both L and M cones (Calkins & Sterling, 1996). The "random connection" hypothesis (Lennie, 1980; Paulus & Kroger-Paulus, 1983; Shapley & Perry, 1986; Lennie et al., 1991; Mullen & Kingdom, 1996) shows that opponency can exist even when the surround gets indiscriminate L and M cone inputs because even mixed surrounds get a substantial contribution from the cone type not mediating the center response. This contribution has been shown to be sufficient to produce opponency in the surrounds (1/e receptive field diameter of ~21 μm) of foveal midget ganglion cells (Lennie et al., 1991).

Our finding that H1 receptive fields are relatively small and get a strong direct cone input combined with recent evidence that L and M cones are randomly distributed in the photoreceptor mosaic (Mollon & Bowmaker, 1992; Packer et al., 1996; Roorda et al., 2001) suggests that midget cell surrounds may be less homogenous than originally thought. The weak surround proposed for the mixed surround model samples many L and M cones and assigns them similar weight, resulting in homogeneous surrounds with the same relative numbers of L and M cones as exist in the mosaic as a whole. When the relative numbers of L and M cones are similar, this model predicts good opponency regardless of which cone type provides input to the center of the receptive field. However, if the cone ratio is substantially different than 1, it becomes difficult to get good opponency for those receptive fields getting center input from the more numerous cone type. If, on the other hand, small receptive fields whose centralmost cones are heavily weighted sample a patchy mosaic, a whole range of chromatic signatures results. Some H1 cells sample a patch of L cones, others sample a patch of M cones, many others sample mixed L and M cones over a range of ratios. Likewise, the receptive fields whose surrounds are mediated by these H1 cells would range from highly opponent to completely nonopponent with a large range in between.

To explore the effects of this modified surround organization, we created a geometric model of the cone and H1 mosaics, similar to the initial stages of previous models (Lennie et al., 1991; Mullen & Kingdom, 1996), to calculate the expected strength of L and M cone input to H1 and midget bipolar cells. A triangular lattice of cones (Figure 13a) was assigned an L /M ratio of 1.5:1 (Dacey, Diller, et al., 2000; Roorda et al., 2001; Jacobs & Deegan, 1997; Packer et al., 1996). Otherwise, L and M cones were assigned randomly. An array of H1 receptive fields (Figure 13a, large circles) sampled the cone mosaic. Each receptive field had a peak sensitivity that decreased exponentially away from the receptive field center. The L (M) cone input to each H1 cell was the sum of the scaled sensitivities of the L (M) cones that fell within its receptive field. Finally, bipolar cells (not shown) positioned at the locations of the cones got center input from the cones directly above them. Surround input was calculated by summing the L and M cone inputs to the single H1cell mediating the surround.

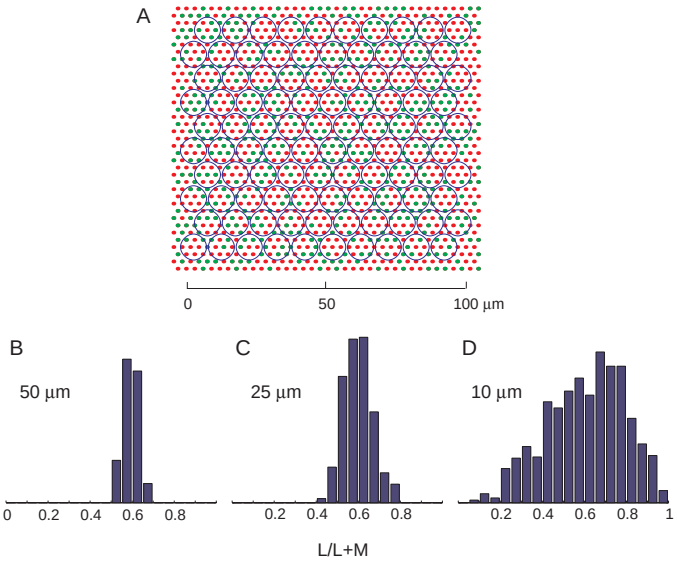

Figure 13. A simple geometrical model for calculating the L and M cone inputs to the surrounds of midget bipolar cells. a. A schematic of the retinal anatomy of the model. The small red and green dots represent L and M cones. The large circles are the receptive field diameters of the H1 cells. Each H1 cell gets input from the cones enclosed by its receptive field. b. A histogram of the relative L and M cone input, expressed as the ratio L/L+M, to the surrounds of bipolar cells getting surround input from a single H1 cell with a receptive field 50 µm in diameter. On this scale, pure M cone input is represented by a ratio of 0.0, whereas pure L cone input is represented by a ratio of 1.0. c. The same as "b" except that H1 receptive field diameter was 25 µm. d. The same as "b" except that H1 receptive field diameter was 10 µm.

When H1 receptive field diameter was 50µm (Figure 13b), slightly larger than the smallest H1 receptive field that we measured, all of the resulting bipolar surrounds had a narrow range of L/L+M ratios (0.5 to 0.7) centered on the ratio of the cone mosaic as a whole (0.6). Foveal H1 receptive field diameters of 25 µm, (Figure 13c), probably the smallest that exist, produced a wider range of ratios (0.4 to 0.8). When receptive field diameter was reduced to 10 µm (Figure 13d), smaller than any H1 receptive field or ganglion cell surround, the range of ratios expanded sufficiently to include a few cells with pure cone input. This result suggests that a relatively homogeneous surround of mixed L and M cone input provides sufficient opponency without much additional sharpening. Some people have highly asymmetric L and M cone ratios but otherwise normal color vision (Vimal, Pokorny, Smith, & Shevell, 1989; Wesner, Pokorny, Shevell, & Smith, 1991). Combined with the finding that the cone input ratios of ganglion cells match those of the H1 cells (Diller, Verweij, Williams, & Dacey, 1999), this result suggests that additional neural processes, presumably cortical (Brainard et al., 2000), further modify the relative contributions of L and M cones.

Acknowledgments

Supported by National Institutes of Health Grants EY06678, EY09625, EY01730 (Vision Research Core) and RR00166 (Regional Primate Center at the University of Washington). The authors would like to thank Joel Pokorny and Vivianne Smith for helpful comments, Toni Haun for drawing cells, and Beth Peterson for making electrodes and processing retinas. Commercial Relationships: None.

References

Barlow, H. B. (1957). Change of organization in the receptive fields of the cat's retina during dark adaptation. *Journal of Physiology*, *137*, 338-354.

Baylor, D. A., Fuortes, M. G., & O'Bryan, P. M. (1971). Receptive fields of cones in the retina of the turtle. *Journal of Physiology*, *214*, 265-294. [PubMed]

Benardete, E. A., & Kaplan, E. (1997a). The receptive field of the primate P retinal ganglion cell. I. Linear dynamics. *Visual Neuroscience*, *14*, 169-185. [PubMed]

Benardete, E. A., & Kaplan, E. (1997b). The receptive field of the primate P retinal ganglion cell. II. Nonlinear dynamics. *Visual Neuroscience*, *14*, 187-205. [PubMed]

Bloomfield, S. A. (1992). Relationship between receptive and dendritic field size of amacrine cells in the rabbit retina. *Journal of Neurophysiology*, *68*, 711-725. [PubMed]

Bloomfield, S. A., Xin, D., & Persky, S. E. (1995). A comparison of receptive field and tracer coupling size of horizontal cells in the rabbit retina. *Visual Neuroscience*, *12*, 985-999. [PubMed]

Bloomfield, S. A., & Xin, D. (2000). Surround inhibition of mammalian AII amacrine cells is generated in the proximal retina. *Journal of Physiology*, *15*, 771-783. [PubMed]

Brainard, D. H., Roorda, A., Yamauchi, Y., Calderone, J. B., Metha, A., Neitz, M., Neitz, J., Williams, D. R., & Jacobs, G. H. (2000). Functional consequences of the relative numbers of L and M cones. *Journal of the Optical Society of America A*, *7*, 607-614. [PubMed]

Calkins, D. J., Schein, S. J., Tsukamoto, Y., & Sterling, P. (1994). M and L cones in macaque fovea connect to midget ganglion cells by different numbers of excitatory synapses. *Nature*, *371*, 70-72. [PubMed]

Calkins, D. J., & Sterling, P. (1996). Absence of spectrally specific lateral inputs to midget ganglion cells in primate retina. *Nature*, *381*, 613-615. [PubMed]

Croner, L. J., & Kaplan, E. (1995). Receptive fields of P and M ganglion cells across the primate retina. *Vision Research*, *35*, 7-24. [PubMed]

Dacey, D. M. (1999). Origins of spectral opponency in primate retina. In J. Toyoda, M. Murakami, A. Kaneko, T. Saito (Eds.), *The retinal basis of vision* (pp. 215-230). Amsterdam: Elsevier.

Dacey, D. M., Diller, L. C., Verweij, J., & Williams, D. R. (2000). Physiology of L- and M-cone inputs to H1 horizontal cells in the primate retina. *Journal of the Optical Society of America A*, *17*, 589-596. [PubMed]

Dacey, D. M., & Lee, B. B. (1994). The 'blue-on' opponent pathway in primate retina originates from a distinct bistratified ganglion cell type. *Nature*, *367*, 731-735. [PubMed]

Dacey, D. M., Lee, B. B., Stafford, D. K., Pokorny, J., & Smith, V. C. (1996). Horizontal cells of the primate retina: Cone specificity without spectral opponency. *Science*, *271*, 656-659. [PubMed]

Dacey, D., Packer, O. S., Diller, L., Brainard, D., Peterson, B., & Lee, B. (2000). Center surround receptive field structure of cone bipolar cells in primate retina. *Vision Research*, *40*, 1801-1811. [PubMed]

Dacheux, R. F., & Raviola, E. (1990). Physiology of HI horizontal cells in the primate retina. *Proceeding of the Royal Society of London B Biological Sciences*, *239*, 213-230. [PubMed]

Demb, J. B., Haarsma, L., Freed, M. A., & Sterling, P. (1999). Functional circuitry of the retinal ganglion cell's nonlinear receptive field. *Journal of Neuroscience*, *19*, 9756-9767. [PubMed]

de Monasterio, F. M. (1978). Center and surround mechanisms of opponent-color X and Y ganglion cells of retina of macaques. *Journal of Neurophysiology*, *41*, 1418-1434. [PubMed]

Diller, L. C., Verweij, J., Williams, D. R., & Dacey, D. M. (1999). L and M cone inputs to peripheral parasol and midget ganglion cells in primate retina. *Investigative Ophthalmology and Visual Science*, *40*, S817.

Enroth-Cugell, C., Robson, J. G., Schweitzer-Tong, D. E., & Watson, A. B. (1983). Spatio-temporal interactions in cat retinal ganglion cells showing linear spatial summation. *Journal of Physiology*, *341*, 279-307. [PubMed]

Euler, T., & Masland, R. H. (2000). Light-evoked responses of bipolar cells in a mammalian retina. *Journal of Neurophysiology*, *83*, 1817-1829. [PubMed]

Flores-Herr, N., Protti, D. A., & Wässle, H. (2001). Synaptic currents generating the inhibitory surround of ganglion cells in the mammalian retina. *Journal of Neuroscience 21*, 4852-4863. [PubMed]

Hidaka, S., Maehara, M., Umino, O., Lu, Y., & Hashimoto, Y. (1993). Lateral gap junction connections between retinal amacrine cells summating sustained responses. *Neuroreport*, *5*, 29-32. [PubMed]

Hochstein, S., & Shapley, R. M. (1976). Linear and nonlinear spatial subunits in Y cat retinal ganglion cells. *Journal of Physiology*, *262*, 265-284. [PubMed]

Jacobs, G. H., & Deegan, J. F. (1997). Spectral sensitivity of macaque monkeys measured with ERG flicker photometry. *Visual Neuroscience, 14*, 921-928. [PubMed]

Kamermans, M., Fahrenfort, I., Schultz, K., Janssen-Bienhold, U., Sjoerdsma, T., & Weiler, R. (2001). Hemichannel-mediated inhibition in the outer retina. *Science*, *292*, 1178-1180. [PubMed]

Kamermans, M., & Spekreijse, H. (1999). The feedback pathway from horizontal cells to cones: A mini review with a look ahead. *Vision Research*, *39*, 2449-2468. [PubMed]

Kaneko, A. (1970). Physiological and morphological identification of horizontal, bipolar and amacrine cells in goldfish retina. *Journal of Physiology*, *207*, 623-633. [PubMed]

Kaneko, A. (1971). Electrical connexions between horizontal cells in the dogfish retina. *Journal of Physiology*, *213*, 95-105. [PubMed]

Kaplan, E., & Benardete, E. (2001). The dynamics of primate retinal ganglion cells. *Progress in Brain Research*, *134*, 17-34. [PubMed]

Kaplan, E., & Shapley, R. M. (1982). X and Y cells in the lateral geniculate nucleus of macaque monkeys. *Journal of Physiology*, *330*, 125-143. [PubMed]

Kirsch, M., & Wagner, H. J. (1989). Release pattern of endogenous dopamine in teleost retinae during light adaptation and pharmacological stimulation. *Vision Research*, *29*, 147-154. [PubMed]

Kolb, H., & Dekorver, L. (1991). Midget ganglion cells of the parafovea of the human retina: A study by electron microscopy and serial section reconstructions. *Journal of Comparative Neurology*, *303*, 617-636. [PubMed]

Lamb, T. D. (1976). Spatial properties of horizontal cell responses in the turtle retina. *Journal of Physiology*, *263*, 239-255. [PubMed]

Lankheet, M. J., Frens, M. A., & van de Grind, W. A. (1990). Spatial properties of horizontal cell responses in the cat retina. *Vision Research*, *30*, 1257-1275. [PubMed]

Lankheet, M. J., Lennie, P., & Krauskopf, J. (1998). Distinctive characteristics of subclasses of red-green P-cells in LGN of macaque. *Visual Neuroscience*, *15*, 37-46. [PubMed]

Lankheet, M. J., Prickaerts, J. H., & van de Grind, W. A. (1992). Responses of cat horizontal cells to sinusoidal gratings. *Vision Research*, *32*, 997-1008. [PubMed]

Lee, B. B., Kremers, J., & Yeh, T. (1998). Receptive fields of primate retinal ganglion cells studied with a novel technique. *Visual Neuroscience*, *15*, 161-175. [PubMed]

Lennie, P. (1980). Parallel visual pathways: A review. *Vision Research*, *20*, 561-594. [PubMed]

Lennie, P., Haake, P. W., & Williams, D. R. (1991). The design of chromatically opponent receptive fields. In M.S. Landy, J.A. Movshon (Eds.), *Computational models of visual processing* (pp. 71-82). Cambridge: MIT Press.

Mangel, S. C. (1991). Analysis of the horizontal cell contribution to the receptive field surround of ganglion cells in the rabbit retina. *Journal of Physiology*, *442*, 211-234. [PubMed]

McMahon, M. J., Lankheet, M. J., Lennie, P., & Williams, D. R. (2000). Fine structure of parvocellular receptive fields in the primate fovea revealed by laser interferometry. *Journal of Neuroscience, 20*, 2043-2053. [PubMed]

Mills, S. L., & Massey, S. C. (1994). Distribution and coverage of A- and B-type horizontal cells stained with Neurobiotin in the rabbit retina. *Visual Neuroscience*, *11*, 549-560. [PubMed]

Mills, S. L., & Massey, S. C. (1998). The kinetics of tracer movement through homologous gap junctions in the rabbit retina. *Visual Neuroscience*, *15*, 765-777. [PubMed]

Mills, S. L., & Massey, S. C. (2000). A series of biotinylated tracers distinguishes three types of gap junction in retina. *Journal of Neuroscience, 20*, 8629-8636. [PubMed]

Mollon, J. D., & Bowmaker, J. K. (1992). The spatial arrangement of cones in the primate fovea. *Nature*, *360*, 677-679. [PubMed]

Mullen, K. T., & Kingdom, F. A. (1996). Losses in peripheral colour sensitivity predicted from "hit and miss" post-receptoral cone connections. *Vision Research*, *36*, 1995-2000. [PubMed]

Naka, K. I., & Nye, P. W. (1971). Role of horizontal cells in organization of the catfish retinal receptive field. *Journal of Neurophysiology*, *34*, 785-801. [PubMed]

Naka, K. I., & Rushton, W. A. (1967). The generation and spread of S-potentials in fish (Cyprinidae). *Journal of Physiology*, *192*, 437-461. [PubMed]

Naka, K. I., & Witkovsky, P. (1972). Dogfish ganglion cell discharge resulting from extrinsic polarization of the horizontal cells. *Journal of Physiology*, *223*, 449-460. [PubMed]

Nelson, R. (1977). Cat cones have rod input: A comparison of the response properties of cones and horizontal cell bodies in the retina of the cat. *Journal of Comparative Neurology*, *172*, 109-135.

Packer, O. S., & Dacey, D. M. (2001). Spatial frequency of macaque H1 horizontal cells depends on the relative strength of direct and coupled inputs. *Investigative Ophthalmology and Visual Science*, *42*, S509.

Packer, O., Diller, L. C., Verweij, J., Lee, B. B., Pokorny, J., Williams, D. R., Dacey, D. M., & Brainard, D. H. (2001). Characterization and use of a digital light projector for vision research. *Vision Research*, *41*, 427-439. [PubMed]

Packer, O. S., Williams, D. R., & Bensinger, D. G. (1996). Photopigment transmittance imaging of the primate photoreceptor mosaic. *Journal of Neuroscience*, *16*, 2251-2260. [PubMed]

Paulus, W., & Kroger-Paulus, A. (1983). A new concept of retinal colour coding. *Vision Research*, *23*, 529-540. [PubMed]

Peichl, L., & Wässle, H. (1983). The structural correlate of the receptive field centre of alpha ganglion cells in the cat retina. *Journal of Physiology*, *341*, 309-324. [PubMed]

Peters, B. N., & Masland, R. H. (1996). Responses to light of starburst amacrine cells. *Journal of Neurophysiology*, *75*, 469-480. [PubMed]

Piccolino, M., Neyton, J., & Gerschenfeld, H. M. (1984). Decrease of gap junction permeability induced by dopamine and cyclic adenosine 3':5'-monophosphate in horizontal cells of turtle retina. *Journal of Neuroscience*, *4*, 2477-2488. [PubMed]

Polyak, S. L. (1941). *The retina.* Chicago: University of Chicago Press.

Pottek, M., & Weiler, R. (2000). Light-adaptive effects of retinoic acid on receptive field properties of retinal horizontal cells. *European Journal of Neuroscience*, *12*, 437-445. [PubMed]

Rall, W. (1959). Branching dendritic trees and motoneuron membrane resistivity. *Experimental Neurology*, *2*, 503-532.

Reid, R. C., & Shapley, R. M. (1992). Spatial structure of cone inputs to receptive fields in primate lateral geniculate nucleus. *Nature*, *356*, 716-718. [PubMed]

Roorda, A., Metha, A. B., Lennie, P., & Williams, D. R. (2001). Packing arrangement of the three cone classes in primate retina. *Vision Research*, *41*, 1291-1306. [PubMed]

Shannon, C. E. (1949). Communication in the presence of noise. *Proceedings of the Institute of Radio Engineers*, *37*, 10-21.

Shapley, R. M., & Perry, V. H. (1986). Cat and monkey retinal ganglion cells and their visual functional roles. *Trends in Neuroscience*, *9*, 229-235.

Smith,V. C., Lee, B. B., Pokorny, J., Martin, P. R., & Valberg, A. (1992). Responses of macaque ganglion cells to the relative phase of heterochromatically modulated lights. *Journal of Physiology*, *458*, 191-221. [PubMed]

Smith, V. C., Pokorny, J., Lee, B. B., & Dacey, D. M. (2001). Primate horizontal cell dynamics: An analysis of sensitivity regulation in the outer retina. *Journal of Neurophysiology*, *85*, 545-558. [PubMed]

Soodak, R. E., Shapley, R. M., & Kaplan, E. (1991). Fine structure of receptive-field centers of X and Y cells of the cat. *Visual Neuroscience*, *6*, 621-628. [PubMed]

Stafford, D. K., & Dacey, D. M. (1997). Physiology of the A1 amacrine: A spiking, axon-bearing interneuron of the macaque monkey retina. *Visual Neuroscience*, *4*, 507-522.

Taylor, W. R. (1996). Response properties of long-range axon-bearing amacrine cells in the dark-adapted rabbit retina. *Visual Neuroscience*, *13*, 599-604. [PubMed]

Taylor, W. R. (1999). TTX attenuates surround inhibition in rabbit retinal ganglion cells. *Visual Neuroscience*, *16*, 285-290. [PubMed]

Taylor, W. R., & Wässle, H. (1995). Receptive field properties of starburst cholinergic amacrine cells in the rabbit retina. *European Journal of Neuroscience*, *7*, 2308-2321. [PubMed]

Teranishi T., & Negishi K. (1994). Double-staining of horizontal and amacrine cells by intracellular injection with lucifer yellow and biocytin in carp retina. *Neuroscience*, *59*, 217-226. [PubMed]

Thibos, L. N. (2000). Formation and sampling of the retinal image. In K. K. De Valois (Ed.), *Seeing* (pp. 1-54). London: Academic Press.

Thibos, L. N., & Levick, W. R. (1983). Spatial frequency characteristics of brisk and sluggish ganglion cells of the cat's retina. *Experimental Brain Research*, *51*, 16-22.

Tomita, T. (1965). Electrophysiological study of the mechanisms subserving color coding in the fish retina. *Cold Spring Harbor Symposium in Quantitative Biology*, *30*, 559-566.

Tornqvist, K., Yang, X. L., & Dowling, J. E. (1988). Modulation of cone horizontal cell activity in the teleost fish retina. III. Effects of prolonged darkness and dopamine on electrical coupling between horizontal cells. *Journal of Neuroscience*, *8*, 2279-2288. [PubMed]

Vaney, D. I. (1994). Patterns of neuronal coupling in the retina. *Progress in Retinal Research*, *13*, 301-355.

Verweij, J., Dacey, D. M., Peterson, B. B., & Buck, S. L. (1999). Sensitivity and dynamics of rod signals in H1 horizontal cells of the macaque monkey retina. *Vision Research*, *39*, 3662-3672. [PubMed]

Vimal, R. L., Pokorny, J., Smith, V. C., & Shevell, S. K. (1989). Foveal cone thresholds. *Vision Research*, *29*, 61-78. [PubMed]

Wässle, H., Boycott, B. B., & Rohrenbeck, J. (1989). Horizontal cells in the monkey retina: Cone connections and dendritic network. *European Journal of Neuroscience*, *1*, 421-435.

Wässle, H., Dacey, D. M., Haun, T., Haverkamp, S., Grunert, U., & Boycott, B. B. (2000). The mosaic of horizontal cells in the macaque monkey retina: With a comment on biplexiform ganglion cells. *Visual Neuroscience*, *17*, 591-608. [PubMed]

Watanabe, M., & Rodieck, R. W. (1989). Parasol and midget ganglion cells of the primate retina. *Journal of Comparative Neurology*, *289*, 434-454. [PubMed]

Werblin, F. S., & Dowling, J. E. (1969). Organization of the retina of the mudpuppy, *Necturus maculosus*. II. Intracellular recording. *Journal of Neurophysiology*, *32*, 339-355. [PubMed]

Wesner, M. F., Pokorny, J., Shevell, S. K., & Smith, V. C. (1991). Foveal cone detection statistics in color-normals and dichromats. *Vision Research*, *31*, 1021-1037. [PubMed]

Williams, D. R. (1985). Aliasing in human foveal vision. *Vision Research*, *25*, 195-205. [PubMed]

Williams, D. R. (1988). Topography of the foveal cone mosaic in the living human retina. *Vision Research*, *28*, 433-454. [PubMed]

Witkovsky, P., Owen, W. G., & Woodworth, M. (1983). Gap junctions among the perikarya, dendrites, and axon terminals of the luminosity-type horizontal cell of the turtle retina. *Journal of Comparative Neurology*, *216*, 359-368. [PubMed]

Yamada, E., & Ishikawa, T. (1965). The fine structure of the horizontal cells in some vertebrate retinae. *Cold Spring Harbor Symposium in Quantitative Biology*, *30*, 383-392.

Yamada, M., Yasui, S., Furukawa, T., Petruv, R., & Djamgoz, M. B. A. (1995). Control of receptive field size in retinal horizontal cells: Direct modulation of gap junction conductance and plasticity of photoreceptor synaptic input. *Progress in Cell Research*, *4*, 269-272.

Yang, G., & Masland, R. H. (1994). Receptive fields and dendritic structure of directionally selective retinal ganglion cells. *Journal of Neuroscience*, *14*, 5267-5280. [PubMed]